RSC Advances

PAPER

View Article Online
View Journal | View Issue

Cite this: *RSC Adv.*, 2024, **14**, 3888

Construction of Z-scheme AgCl/BiOCl heterojunction with oxygen vacancies for improved pollutant degradation and bacterial inactivation

Shuai Fu, †*[ab] Zhiliang Chu,†[c] Zhiquan Huang,[ab] Xiaomei Dong,[a] Junhong Bie,[d] Zhe Yang,[ab] Huijie Zhu, *[ab] Wanyu Pu,[a] Wanzhe Wu[a] and Bo Liu[e]

A facile Z-scheme AgCl/BiOCl heterojunction photocatalyst with oxygen vacancies was fabricated by a water-bath method. The structural, morphological, optical and electronic properties of as-synthesized samples were systematically characterized. The oxygen vacancies were confirmed by EPR, which could optimize the band-gap of the AgCl/BiOCl heterojunction and improve the photo-induced electron transfer. The optimized AgCl/BiOCl heterojunction showed excellent photocatalytic degradation efficiency (82%) for tetracycline (TC). Simultaneously, *E. coli* was completely inactivated within 60 min due to the AgCl/BiOCl heterojunction. The elevated catalytic activity of the optimal AgCl/BiOCl heterojunction was ascribed to the synergistic effect of the enhanced light absorption and effective photoinduced charge carrier separation and transfer. Moreover, the degradation efficiency of the AgCl/BiOCl heterojunction towards ofloxacin, norfloxacin and Lanasol Red 5B was 73%, 74% and 96%, respectively. The experimental factors for the degradation efficiency of TC were also studied. Furthermore, active species trapping experiments indicated that superoxide radicals ($^{\bullet}O_2^-$) were the main reactive species, and the Z-scheme charge transfer mechanism helped to improve the photocatalytic activity.

Received 13th December 2023
Accepted 16th January 2024

DOI: 10.1039/d3ra08514g

rsc.li/rsc-advances

1 Introduction

Tetracycline hydrochloride, a member of the tetracycline antibiotic class, can have extremely strong toxicity in water. When tetracycline is released into water, it can persist and accumulate due to its slow degradation rate, causing harm to aquatic organisms.[1,2] Additionally, tetracycline can potentially enter the food chain as it is absorbed by aquatic organisms, thereby posing risks to higher trophic levels, including fish and other aquatic life and potentially affecting human health through consumption. It is extraordinarily important to manage and regulate the use and disposal of tetracycline to minimize its adverse effects on water bodies. In addition, one of the most important effects of pathogenic microorganisms on humans is the prevalence of infectious diseases.[3] *Escherichia coli*, *Staphylococcus aureus* and *Salmonella* are common pathogenic bacteria in water. Traditional technologies often produce toxic by-products during the antibacterial process, causing secondary pollution. Therefore, researchers have tried to use new technology to inhibit bacteria.[4,5] As it is well-known, photocatalysis is a kind of water treatment technology with high efficiency, high mineralization rate, and low cost, which provides a good strategy for tetracycline removal and bacterial inactivation.[6–8]

Bismuth oxychloride (BiOCl) is one of the ternary bismuth-based semiconductors with a special layered structure.[9–11] Its special structure is composed of $[Bi_2O_2]^{2+}$ layers and staggered halide element ions. The alternating arrangement of $[Cl_2]^{2-}$ layers and $[Bi_2O_2]^{2+}$ leads to the generation of an internal electric field that expands its internal space and is distributed along the layers.[12–14] The combined effect of electronegativity differences promotes the polarization of atoms and orbitals related to the reaction, which could achieve efficient separation of photo-induced charge carriers in specific spaces.[15,16] As it is well-known, BiOCl is an indirect semiconductor with a wide bandgap and low utilization of sunlight. More precisely, it is a UV-driven catalyst.[17,18] If it is to be put into mass production and use, the requirements are strict. Its degradation effect can only be maximized when an external UV light source is applied.

[a]*Henan International Joint Laboratory of New Civil Engineering Structure, College of Civil Engineering, Luoyang Institute of Science and Technology, Luoyang 471023, Henan, PR China. E-mail: shuaifu16@163.com; huijiezhu@lit.edu.cn*

[b]*Henan Engineering Research Center of Water Quality Safety in the Middle-lower Yellow River, Henan Green Technology Innovation Demonstration Base, Luoyang 471023, Henan, PR China*

[c]*The 989th Hospital, Department of Central Laboratory, Luoyang 471031, Henan, PR China*

[d]*Henan Communications Planning & Design Institute Co., Ltd, Zhengzhou, 450046, Henan, PR China*

[e]*Laboratory of Functional Molecular and Materials, School of Physics and Optoelectronic Engineering, Shandong University of Technology, Zibo, 255000, Shandong, PR China*

† Shuai Fu and Zhiliang Chu contributed equally to this work.

However, external UV light sources are often inconvenient in practical applications, making the degradation system complex. Thus, it is necessary to modify the photocatalyst to absorb visible light, which accounts for a large proportion of sunlight. A great deal of research has been carried out to promote the photoactivity of BiOCl, including metal and non-metal doping,[19–21] morphology control,[22,23] and heterojunction construction.[24–26] Among these strategies, heterojunction construction is appropriate as it can concurrently extend the light absorption and improve the charge separation and transfer.[7,27,28]

Heterojunctions composed of semiconductors with matching band structures can reduce the band-gap width, making the composite material exhibit excellent photocatalytic activity.[29,30] Silver chloride (AgCl), as an efficient photocatalyst, combining the characteristics of metals and semiconductors, exhibits excellent photocatalytic performance.[31–33] However, AgCl frequently suffers from issues such as photo-corrosion and rapid recombination of photo-induced electrons and holes.[34,35] To solve these problems, the strategy of heterojunction construction is usually adopted. For example, Guo[36] and co-workers successfully synthesized a AgCl/Bi_3TaO_7 heterojunction by a hydrothermal and deposition–precipitation process, which showed excellent photocatalytic efficiency toward TC. Liu[37] and co-workers successfully prepared a AgCl/Ag/$MnTiO_3$ construction with improved photocatalytic efficiency.

In this study, a simple water-bath method was used to prepare a AgCl/BiOCl heterojunction. The structure, morphology, and optical and electrical properties of the AgCl/BiOCl heterojunction were systematically investigated. The photocatalytic activity of the AgCl/BiOCl heterojunction under simulated solar irradiation was investigated toward TC and *Escherichia coli*. The effects of environmental factors on the degradation efficiency of TC were investigated. In addition, a probable mechanism was put forward for the enhanced photocatalytic activity.

2 Experimental

2.1. Chemicals

Bismuth nitrate pentahydrate ($Bi(NO_3)_3 \cdot 5H_2O$), silver nitrate ($AgNO_3$), sodium chloride (NaCl) and ethylene glycol ($(CH_2OH)_2$) were purchased from Sinopharm Chemical Reagent (Shanghai, China). Disodium ethylenediaminetetraacetic acid (EDTA-2Na), 1,4-benzoquinone (BQ) and isopropanol (IPA) were purchased from Aladdin Industrial Co. Ltd., China. All chemicals were of analytical reagent (AR) grade. Deionized water was used in all experiments.

2.2. Synthesis of AgCl/BiOCl

The samples were synthesized by a simple water-bath method.[38] Typically, 3 mmol $Bi(NO_3)_3 \cdot 5H_2O$ was dissolved in 45 mL ethylene glycol, stirring continuously for 1 h. Then, 3 mmol $AgNO_3$ was dissolved in 25 mL deionized water and added into the above solution, which was stirred again for 30 min to obtain solution A. Subsequently, 6 mmol of NaCl was dissolved in 25 mL of deionized water and added dropwise to solution A, stirring magnetically for 2 h under water-bath conditions at 90 °C. The final product was centrifuged, rinsed with deionized water several times, and dried at 60 °C for 24 h. Different amounts of $AgNO_3$ were added to obtain different molar ratios (1 : 4, 1 : 3, 1 : 2, and 1 : 1) of AgCl to BiOCl, denoted as 0.25AB, 0.33AB, 0.5AB and AB, respectively. For comparison, AB with poor oxygen vacancies was synthesized using a similar procedure without ethylene glycol and denoted as AB-P.

2.3. Characterization

The crystal phases of as-prepared samples were probed in the 2θ range of 10–80° by X-ray diffraction (XRD) using a Bruker-D8-Axs diffractometer system with Cu Kα radiation (λ = 0.15406 Å). X-ray photoelectron spectroscopy (XPS) was conducted on a Thermo Escalab 250 spectrometer and all binding energy values were calibrated using the C 1s peak at 284.7 eV of the surface adventitious carbon. The morphological details of samples were examined with TEM (JEM-2100) and SEM (SU8010). The optical properties were measured by UV-vis spectrophotometry (PerkinElmer) in the wavelength range of 200–800 nm. The electron paramagnetic resonance (EPR) spectra were acquired on a Bruker ER300-SRC instrument.

2.4. Evaluation of the simulated solar-driven photocatalytic performance

The photocatalytic activities of the prepared AgCl/BiOCl heterojunction were evaluated *via* photodegradation of TC under a 350 W xenon lamp. Typically, a 40 mL aqueous solution containing TC (40 mg L^{-1}) and catalysts (1 g L^{-1}) was agitated for 30 min in the dark to attain adsorption–desorption equilibrium. During the photoreaction, 4 mL of solution was withdrawn at scheduled intervals and centrifuged. The concentration of TC in the supernatant was measured with a UV-vis spectrophotometer (UV-2450). The degradation efficiency was calculated as $(C_0 - C_t)/C_0$, where C_0 is the initial concentration and C_t is the concentration of the pollutant at time t during degradation.

2.5. Bacterial inactivation test

The antimicrobial experiments were conducted with Gram-negative *Escherichia coli* (*E. coli*, ATCC®25922). The prepared photocatalysts were treated with ultrasound for 2 h and subsequently disinfected at 120 °C for 40 min. The catalyst (5 mg L^{-1}) was suspended in a 10 mL *E. coli* culture medium and illuminated under a 350 W xenon lamp. During photocatalytic antimicrobial experiments, 1 mL suspensions were withdrawn at a scheduled interval and solutions were first serially diluted and coated again on solid LB medium. The viable cell density was counted after incubation at 37 °C for 24 h. Each set of experiments was conducted in triplicates and the average was calculated.

3 Results and discussion

3.1. Physicochemical properties

XRD is often used to characterize material composition. Fig. 1 shows the X-ray diffraction patterns of BiOCl, AgCl, and AgCl/

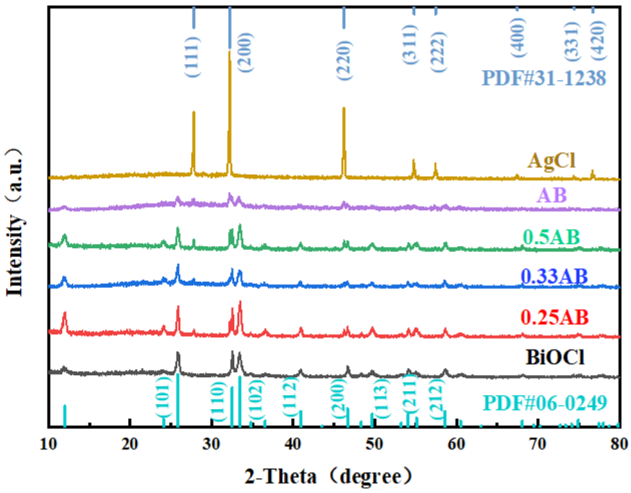

Fig. 1 XRD patterns of the standard diffraction card of AgCl, BiOCl, and AgCl/BiOCl heterojunctions.

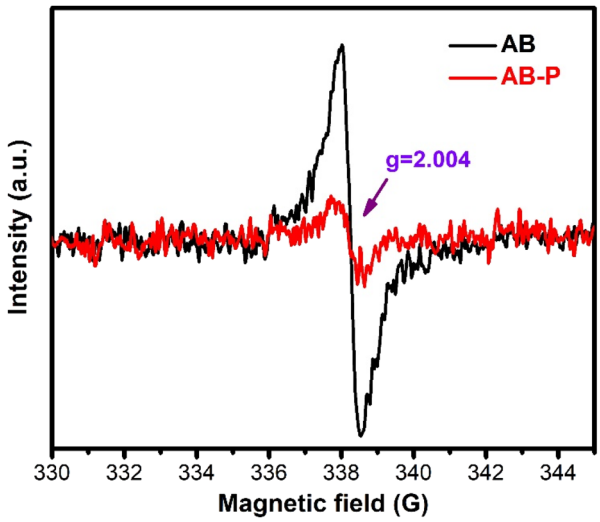

Fig. 2 EPR spectra of as-synthesized AB and AB-P heterostructures.

BiOCl heterojunctions. For BiOCl, predominant characteristic diffraction peaks at 25.8°, 32.5°, 33.4°, 40.8°, 46.6°, 49.7°, 54.1°, and 58.6° correspond to the (101), (110), (102), (112), (200), (113), (211), and (212) crystal planes of tetragonal BiOCl (JCPDS no. 06-0249), respectively.[10] For pure AgCl, the characteristic diffraction peaks at 27.9°, 32.5°, 46.3°, 55.0°, 57.6°, 67.6°, 74.6°, and 76.9° can be indexed to the (111), (200), (220), (311), (222), (400), (331), and (420) crystal planes of AgCl (JCPDS no. 31-1238).[31] Notably, compared with pure BiOCl, the diffraction peaks of the AgCl/BiOCl heterojunction were generally consistent with the tetragonal BiOCl phase. However, with increasing amounts of AgCl, the diffraction peak intensity of BiOCl gradually weakened, and the diffraction peak at $2\theta = 27.9°$, corresponding to the (111) plane of AgCl, was gradually intensified in the AgCl/BiOCl heterojunction. The presence of AgCl did not influence the diffraction peak position of BiOCl, indicating that no obvious chemical reaction occurred at the interface of AgCl and BiOCl. There are no impurity peaks in the spectrum, indicating a high purity of the sample.

As an intrinsic defect, oxygen vacancies (Ovs) significantly affect the electronic structure and physical properties of semiconductors. As shown in Fig. 2, a sharp signal at $g = 2.004$, ascribed to the electron capture of OVs, could confirm that OVs existed in AB.[39] In contrast, a very weak signal was observed from AB-P. The EPR results confirmed the presence of rich OVs in AB. Importantly, photo-induced electrons were trapped by OVs and further reacted with O_2 to generate reactive oxygen species, significantly improving the photocatalytic activity.

The morphology and structure of BiOCl, AgCl, and the AB heterojunction were observed and analyzed by FE-SEM. In Fig. 3a, it can be seen that pure BiOCl was composed of nanosheets with a diameter of 200–500 nm and smooth well-defined surfaces. As shown in Fig. 3b, AgCl exhibited an irregular block structure composed of aggregated particles. After the loading of AgCl, granular AgCl was scattered on the surface of sheet-like BiOCl (Fig. 3c and d), indicating the formation of a AgCl/BiOCl heterojunction, which was beneficial for improving the photocatalytic performance.

The AB heterojunction was further observed by TEM and HRTEM. As shown in Fig. 4a, granular AgCl was deposited on the surface of sheet-like BiOCl in the AB heterojunction. In Fig. 4b, lattice spacings of 0.34 nm and 0.32 nm were observed, which corresponded to the (101) plane of BiOCl and the (111) plane of AgCl, respectively, further proving the successful synthesis of the AgCl/BiOCl heterojunction.

The chemical state and surface elemental composition of AgCl, BiOCl, and the AB heterostructure were confirmed by XPS.[40] Fig. 5a identifies Bi, O, Cl and Ag elements in the AB heterostructure. The peak at 529.92 eV in the O 1s spectrum corresponds to lattice oxygen absorbed on the catalyst surface (Fig. 5b).[41] In Fig. 5c, two peaks at the positions of 198.62 eV and 201.33 eV are attributed to Cl $2p_{3/2}$ and Cl $2p_{1/2}$ of Cl^-, respectively. In the Ag 3d spectrum (Fig. 5d), a double peak was observed at 373.16 eV and 367.20 eV, which could be assigned to Ag $3d_{3/2}$ and Ag $3d_{5/2}$ of Ag^+, respectively.[42]

UV-vis DRS is often used to characterize the optical absorption capacity of semiconductor materials.[43] Fig. 6a shows the spectrum of the synthesized material in the range of 200 nm to 800 nm. The absorption edge of pristine BiOCl was approximately 374 nm. Compared to BiOCl, the light absorption of the AB heterojunction underwent a slight redshift with an absorption edge of 428 nm. The experimental results indicated that the loading of AgCl effectively enhanced the light absorption ability of the AB heterojunction, which helped to improve its photocatalytic performance. The band gap could be calculated from the classic Tauc approach through the equation $\alpha h\nu = A(h\nu - E_g)^{n/2}$,[44] where α, h, ν, A, and E_g are the optical absorption coefficient, Planck's constant, the photon frequency, a constant and the band gap, respectively. According to the fitted band gap, the band gaps of BiOCl, AgCl and the AB heterojunction were estimated to be 3.25 eV, 2.94 eV and 2.70 eV, respectively (Fig. 6b–d). Moreover, Fig. 7a and b show the valence band (VB) positions of the sample measured from VB-XPS spectra,[8]

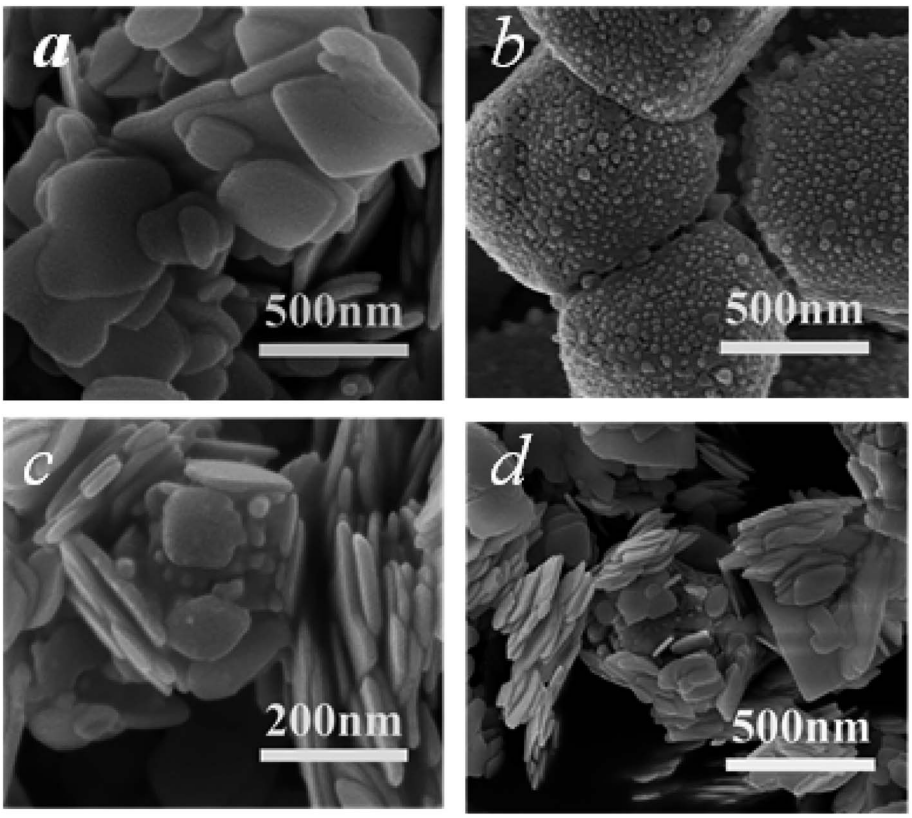

Fig. 3 FE-SEM images of (a) BiOCl, (b) AgCl and (c and d) the AB heterojunction.

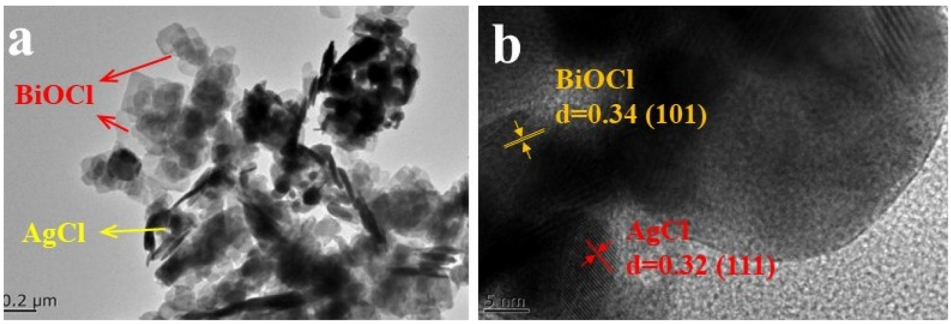

Fig. 4 (a) TEM and (b) HRTEM image of the AB heterojunction.

indicating that the VB positions of BiOCl and AgCl were 3.42 eV and 2.53 eV, respectively. According to the energy band position formula $E_{CB} = E_{VB} - E_g$, the CB positions of BiOCl and AgCl were calculated to be 0.17 eV and −0.41 eV, respectively.

3.2. Photocatalytic activity

For photocatalytic degradation experiments, tetracycline hydrochloride was selected as the target pollutant to evaluate the photocatalytic performance of as-prepared materials. Fig. 8a shows that all AgCl/BiOCl heterojunctions exhibited excellent photocatalytic activity towards TC compared with pure AgCl and BiOCl. Among them, the AB heterojunction showed the best degradation efficiency. After 60 min of simulated solar irradiation, the degradation efficiency of TC reached 82%, which is 1.66 and 2.15 times higher than that of pure BiOCl and AgCl, respectively. In addition, a mechanical mixture of BiOCl and AgCl was tested as a control and exhibited similar photocatalytic activity to BiOCl, which was much lower than that of the hierarchical AgCl/BiOCl heterostructure. This could be attributed to the poor interfacial contact between AgCl and BiOCl during mechanical mixing. As shown in Fig. 8b, the degradation kinetics of TC were fitted using a first-order model. The rate constant of the AB heterojunction was 0.02255 min^{-1}, which was 2.76 and 6.25 times higher than that of BiOCl and AgCl, respectively, indicating that the AB heterojunction had the best photocatalytic activity. These results showed that the formation of the AgCl/BiOCl heterojunction could effectively improve the photocatalytic degradation efficiency of TC.[45]

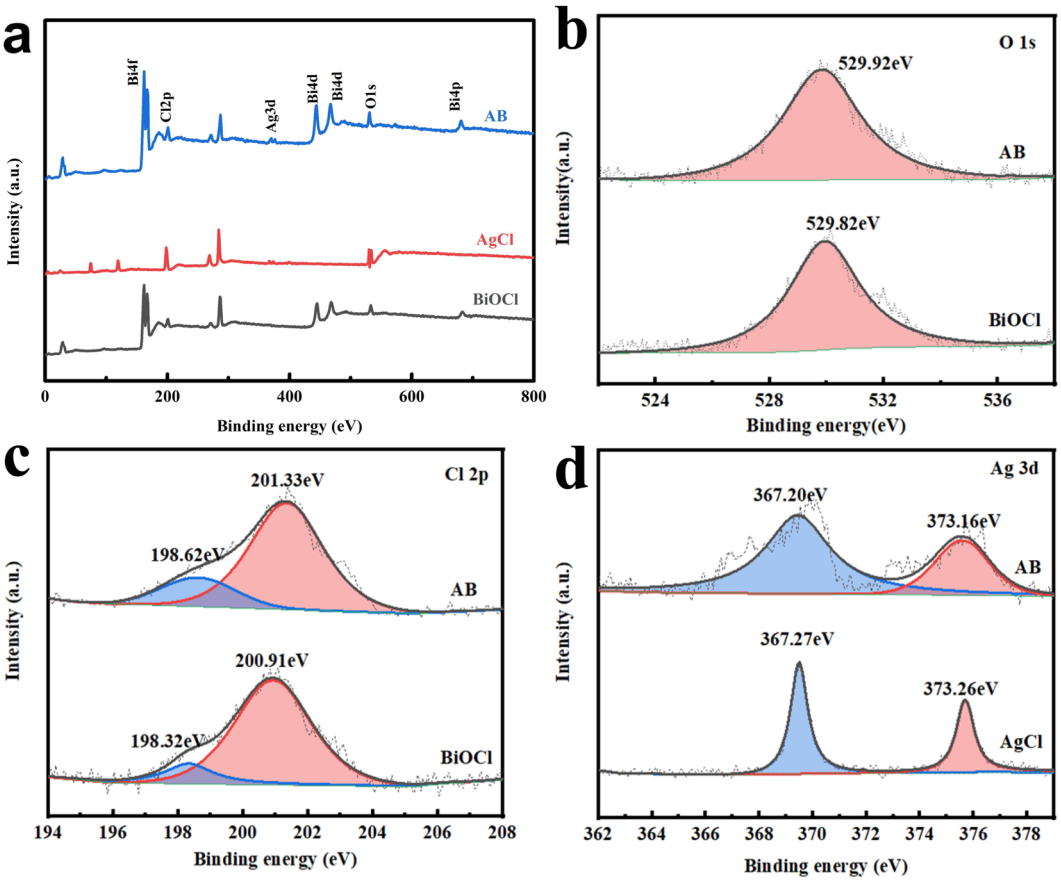

Fig. 5 XPS spectra of AgCl, BiOCl and the AB heterostructure: (a) survey XPS spectra, (b) O 1s, (c) Cl 2p and (d) Ag 3d.

Environmental factors, such as the dosage of photocatalytic material and initial concentration of TC, could have a certain impact on the degradation efficiency. To explore the application of materials in actual wastewater treatment, environmental interference experiments were conducted. Fig. 9a shows the effect of initial concentration of TC on the degradation process. The reaction system consisted of 40 mL of TC solution (pH = 7) with 40 mg of catalyst. When the initial concentration changed from 20–50 mg L^{-1}, the degradation rate of TC decreased from 92% to 79%. As the TC concentration increased, the degradation efficiency gradually decreased, possibly due to the rapid consumption of free radicals produced by the catalyst. Fig. 9b describes the effect of dosage on photocatalytic degradation. When the catalyst dosage increased from 20 mg to 40 mg, the degradation efficiency of TC also increased. However, when the AB heterojunction dosage increased to 60 mg, the improvement of the TC degradation efficiency was not significant. The experimental results indicated that excessive photocatalyst cannot further improve the degradation efficiency, which might be due to the aggregation of photocatalysts and solution turbidity caused by the further increase in catalyst dosage. This would have adverse effects on the exposed specific surface area and active sites, thereby affecting the photocatalytic activity.[46]

The large amount of ions (Cl^-, Cu^{2+}, and PO_4^{3-}) in actual wastewater might affect the photocatalytic degradation activity. As shown in Fig. 10a, the degradation efficiencies of the AB heterojunction towards TC in the presence of three inorganic salts (Cl^-, Cu^{2+}, and PO_4^{3-}, 0.05 M) were significantly different. Distinctly, the degradation efficiency of TC significantly decreased with the addition of PO_4^{3-}, because PO_4^{3-} could consume photo-induced holes and restrict the degradation process.[47] Additionally, the TC degradation was slightly limited by Cu^{2+}, possibly because TC or its intermediates were prone to combining with Cu^{2+} to constitute more stable metal complexes, and photo-induced electrons were consumed by Cu^{2+} distributed on the AB heterojunction surface, further restraining the generation of superoxide or hydroxyl radicals. However, it could be seen that the degradation of TC was little impacted after the addition of Cl^-.[48] The effects of pH on the photocatalytic activities of as-prepared materials are displayed in Fig. 10b. The AB heterojunction had the highest degradation efficiency of TC at pH 7. Under acidic conditions, the degradation efficiency of TC decreased with decreasing pH, which would lead to electrostatic repulsion between the positively charged photocatalyst surface and protonated TC molecules, weakening the adsorption of TC on the AB heterojunction and resulting in a decrease in photocatalytic degradation efficiency. Under alkaline conditions, as the alkalinity increased, the degradation efficiency of TC gradually decreased. When pH was at 9, the degradation efficiency of TC slightly decreased. When the pH increased to 11, the degradation efficiency of TC significantly decreased. This

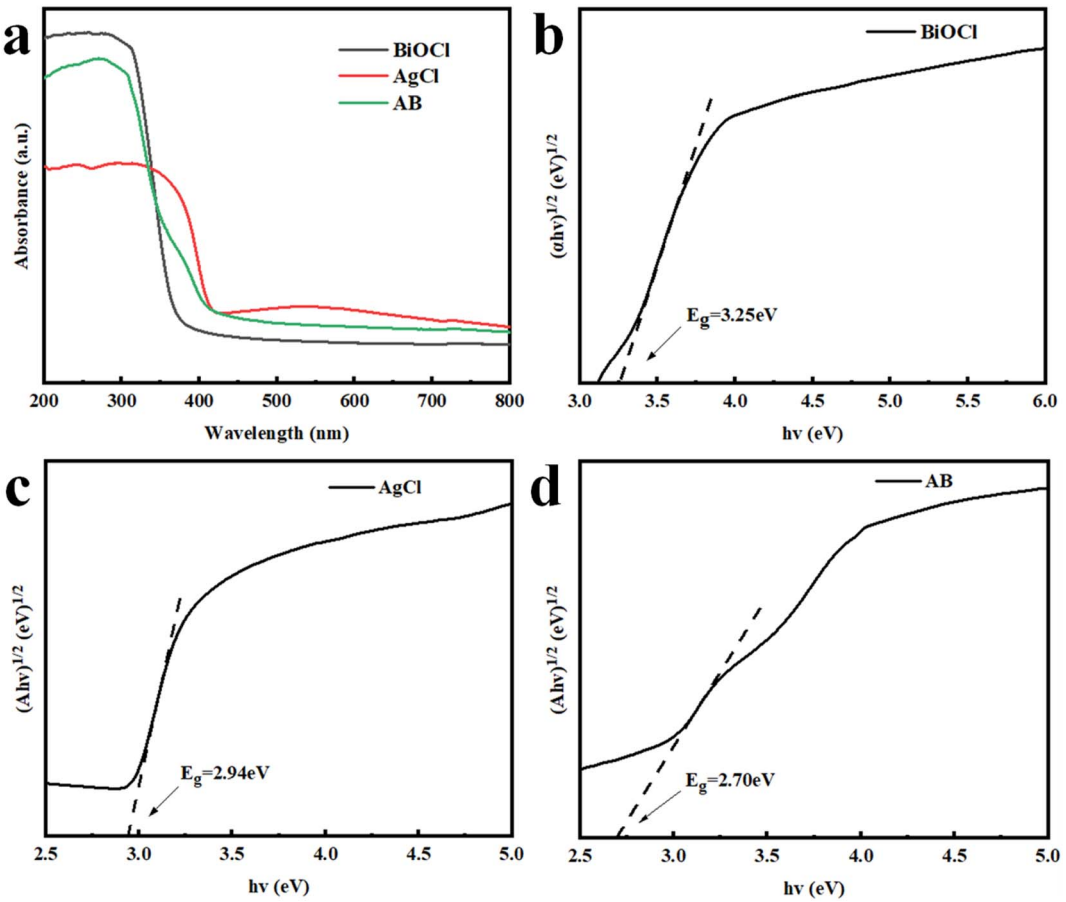

Fig. 6 (a) UV-vis spectra and (b–d) band gap energies of AgCl, BiOCl and the AB heterostructure.

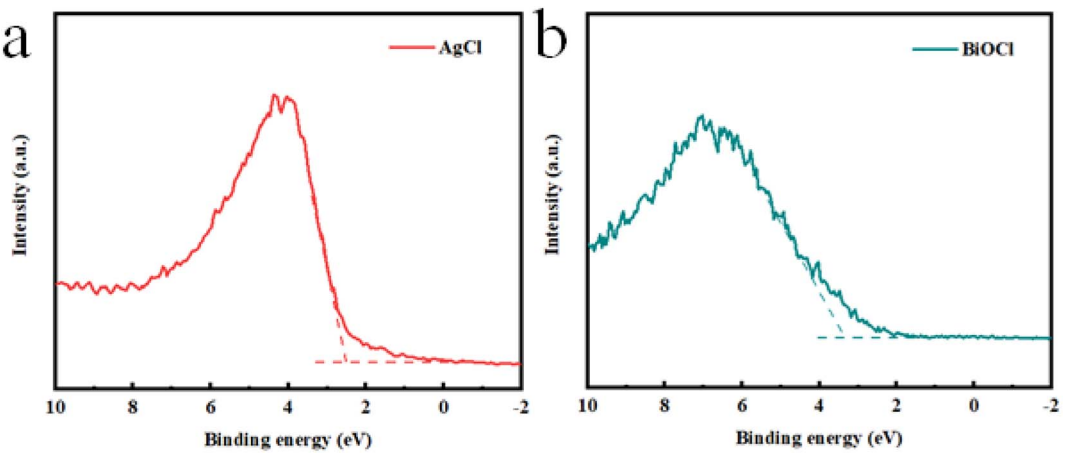

Fig. 7 Valence-band XPS spectra of AgCl (a) and BiOCl (b).

might be caused by chemical changes in the AB heterojunction under alkaline conditions.

To investigate the degradation activity of the AB heterojunction towards different organic pollutants, several molecules like ofloxacin, norfloxacin, and Lanasol Red 5B were tested and their degradation efficiencies were obtained. As shown in Fig. 11a, the photocatalytic degradation efficiencies of ofloxacin, norfloxacin, Lanasol Red 5B and TC were 73.52%, 74.37%, 96.13%, and 81.53%, respectively, under 60 min of simulated solar irradiation. Due to different molecular structures of organic pollutants, the AB heterojunction exhibited distinct photocatalytic performance in the degradation of different organic pollutants.[49] Generally, water environments contain more than one type of organic substance, and the

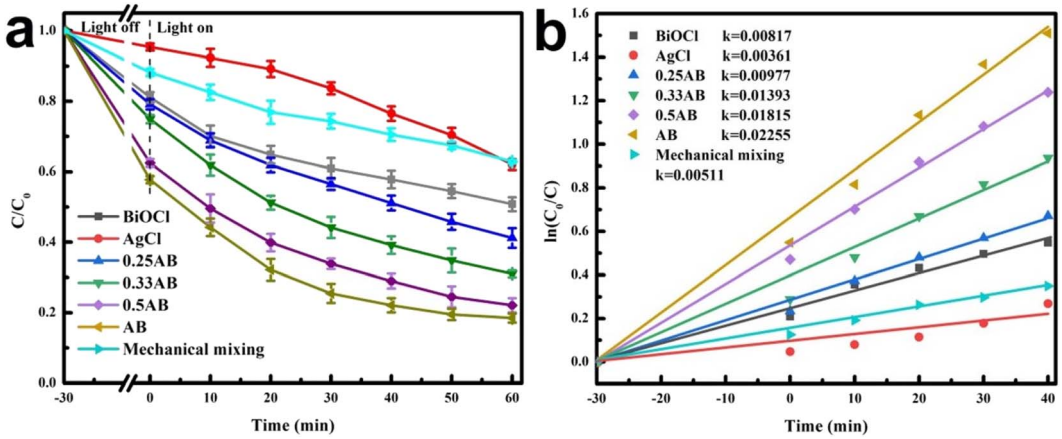

Fig. 8 (a) Degradation efficiencies and (b) kinetic curves of TC using as-prepared photocatalysts under simulated solar irradiation.

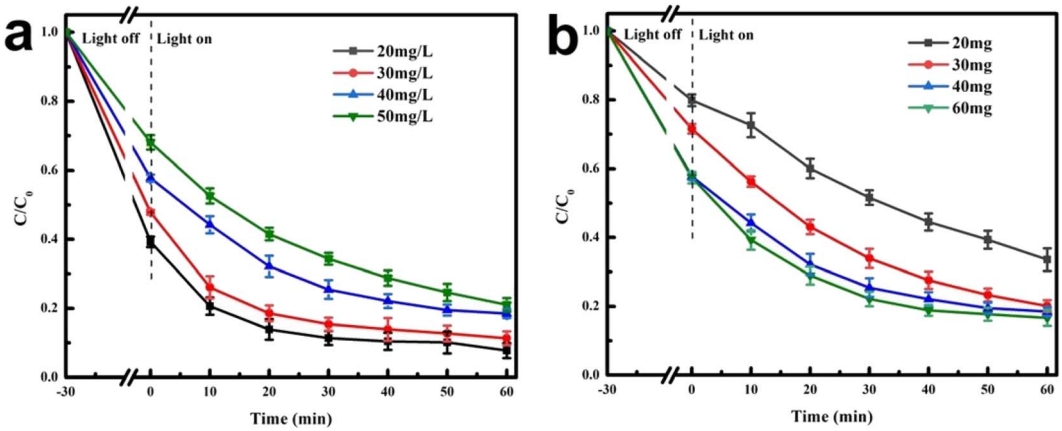

Fig. 9 Efficiencies of (a) different concentrations of TC ([AB] = 40 mg) and (b) different amounts of AB heterojunction ([TC] = 40 mg L^{-1}) under simulated solar irradiation.

coexistence of organic substances will most likely affect the photocatalytic activity of the AB heterojunction. As shown in Fig. 11b, the addition of Lanasol Red 5B significantly inhibited the photocatalytic degradation of TC. After 60 min of simulated solar irradiation, the degradation efficiency of TC was 65.37%, and the degradation efficiency of Lanasol Red 5B was 80.13%. The degradation efficiencies of TC and Lanasol Red 5B declined compared to each alone, which might be due

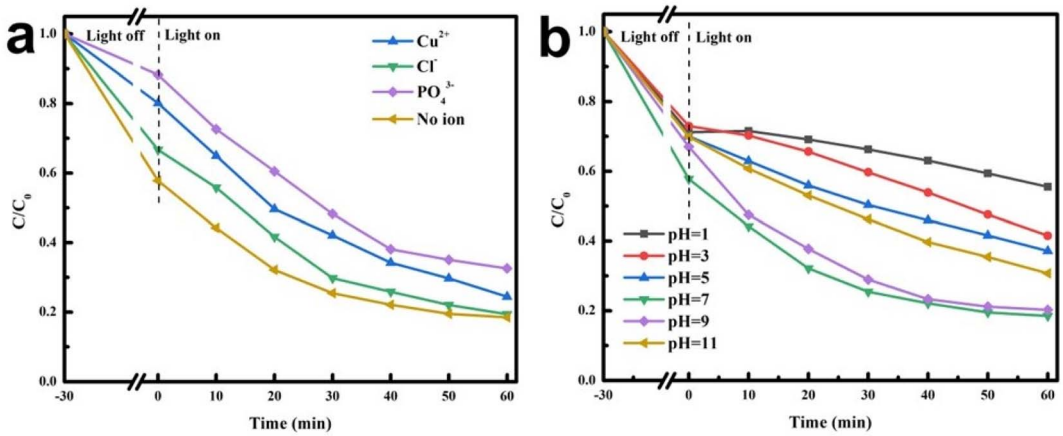

Fig. 10 Degradation efficiencies of TC (a) with different inorganic salts and (b) at different pH.

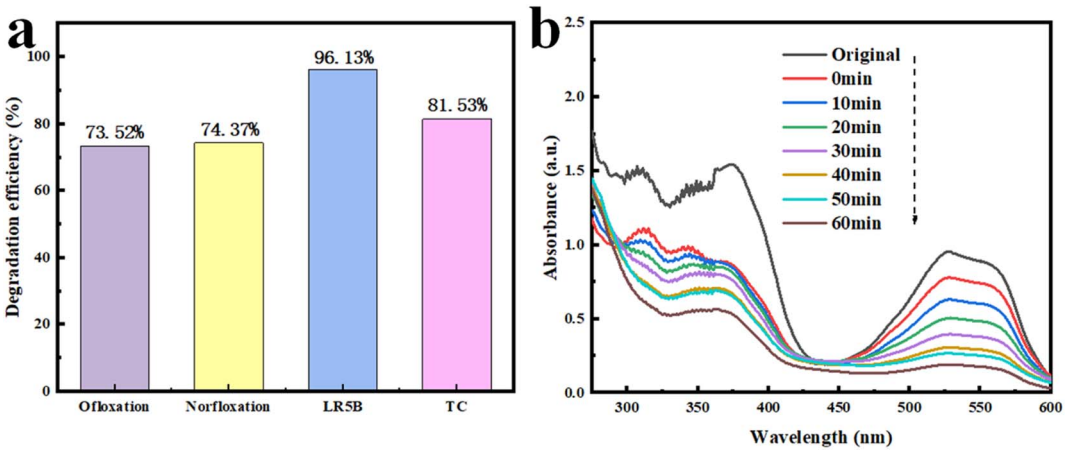

Fig. 11 (a) Degradation efficiencies of ofloxacin, norfloxacin, Lanasol Red 5B and TC. (b) Time-dependent absorption spectra of Lanasol Red 5B and TC.

to the competition between Lanasol Red 5B and TC for active species.

In addition, the effects of lake water and tap water on the TC degradation process were studied. As shown in Fig. 12, the degradation efficiency of TC in tap water and lake water was 79.91% and 75.75%, which was obviously inhibited compared with in deionized water. This was due to the presence of trace amounts of organic substances or ions in tap water and lake water, which consumed active species and led to a decrease of the photocatalytic degradation efficiency.

E. coli was also used as a target bacterium to characterize the photocatalytic sterilization performance.[50] Simulated solar irradiation and BiOCl had almost no effect on killing *E. coli* (Fig. 13g–i). As shown in Fig. 13d–f, pure AgCl showed feeble inactivation ability. When the AB heterojunction was added, it was difficult for *E. coli* to grow, and it was almost completely inactivated after 60 min (Fig. 13a–c). The reason originated from active species, which could damage bacterial cells and kill the *E. coli.*

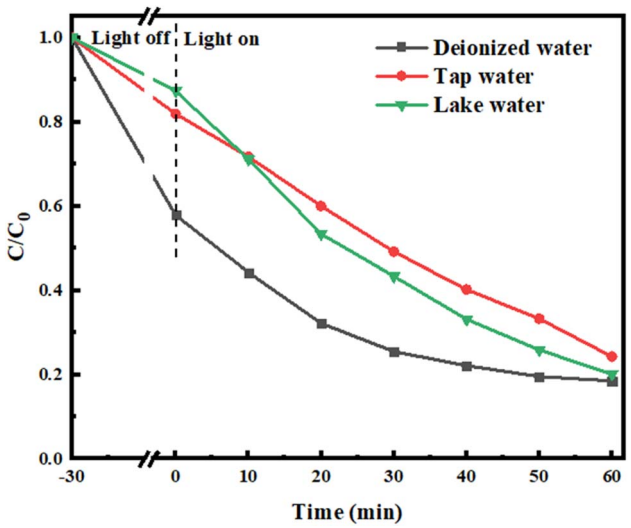

Fig. 12 Degradation efficiencies in different water resources with the AB heterojunction.

3.3. Photocatalytic mechanism

Photoluminescence (PL) spectroscopy was used to investigate the migration and recombination processes of photoinduced electron–hole pairs. Generally, the stronger the fluorescence intensity of the sample, the higher the recombination efficiency of its photo-generated electrons and holes. As shown in Fig. 14a, compared with AgCl and BiOCl, the PL intensity of the AB heterojunction was significantly reduced, indicating that the formation of the AB heterojunction could effectively suppress the recombination of photo-generated carriers.

To preliminarily explore the photocatalytic mechanism of the AgCl/BiOCl heterojunction, different capture agents were added to capture the active species in the reaction system. Fig. 14b shows the degradation efficiency of TC after 60 min of simulated solar irradiation with the addition of *p*-benzoquinone, EDTA-2Na, and isopropanol, respectively. The experimental results showed that EDTA-2Na and isopropanol had a slight impact on the photocatalytic performance of the AB heterojunction, while the photocatalytic activity was significantly inhibited with the addition of benzoquinone. It could be seen that $^{\bullet}O_2^-$ was the main reactive species, while $^{\bullet}OH$ and h^+ played an auxiliary role in the TC degradation process.

Based on the above experimental results, a possible charge transfer mechanism analysis was conducted during the photocatalytic degradation process of the AgCl/BiOCl heterojunction. As shown in Fig. 15a, AgCl and BiOCl surfaces generated photo-induced electron–hole pairs after simulated solar irradiation. According to the traditional charge transfer mechanism (type II), photo-induced electrons on the conduction band of AgCl would transfer to the CB of BiOCl, and photo-induced holes on the valence band of BiOCl would transfer to the VB of AgCl. However, the CB position of BiOCl was +0.17 eV, which was more positive than the standard redox potential of E ($O_2/^{\bullet}O_2^-$) (−0.33 eV *vs.* NHE). Therefore, photogenerated electrons gathered on the surface of BiOCl cannot

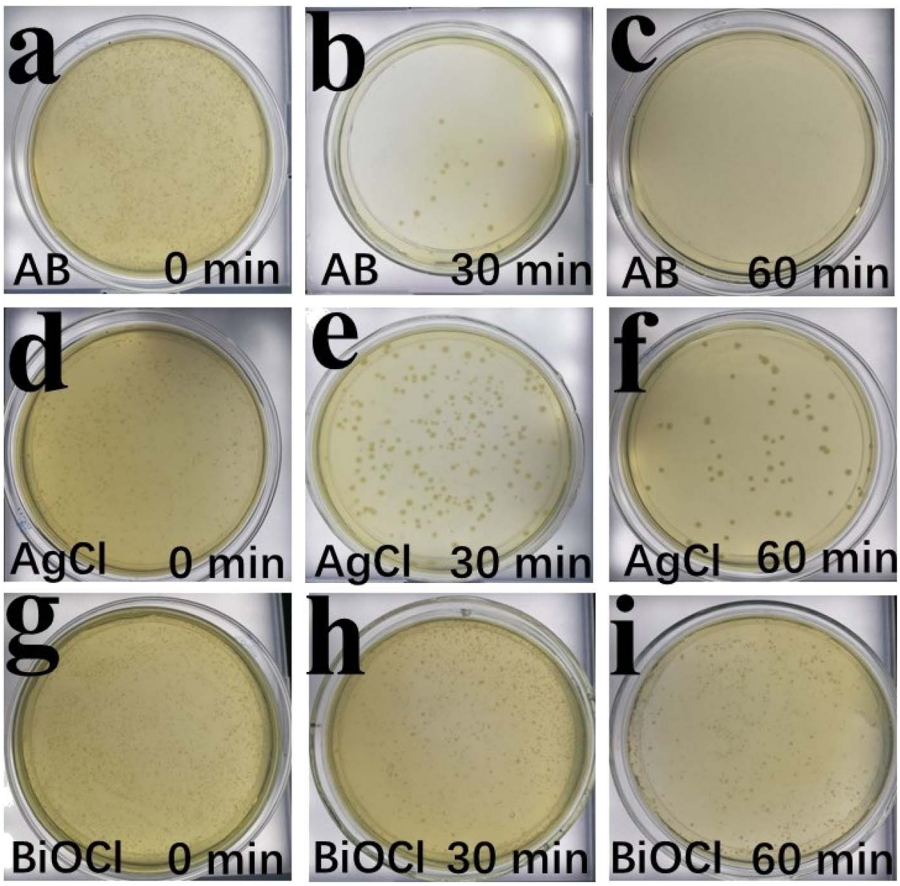

Fig. 13 The surviving culture growth of *E. coli* incubated with as-synthesized samples at fixed time intervals of 0–60 (a–i) min under simulated solar irradiation.

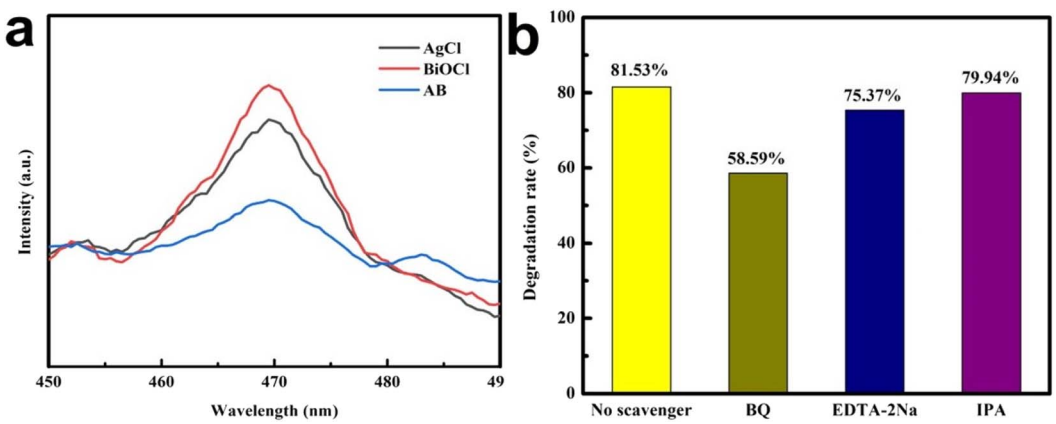

Fig. 14 PL spectra of as-prepared samples (a) and trapping experiment (b).

reduce O_2 to produce $^{\bullet}O_2^-$, which was inconsistent with the capture experiment where $^{\bullet}O_2^-$ was the main active species. Consequently, the Z-scheme charge transfer mechanism was inferred. As shown in Fig. 15b, photo-induced holes on the valence band of AgCl would recombine with photo-induced electrons on the conduction band of BiOCl, thus effectively separating photo-induced electrons and holes. The CB position of AgCl was −0.41 eV, which was more negative than the standard redox potential of E ($O_2/^{\bullet}O_2^-$) (−0.33 eV *vs.* NHE). Therefore, photo-induced electrons on the conduction band of AgCl could reduce O_2 to $^{\bullet}O_2^-$. In addition, the VB position of BiOCl was +3.42 eV, which was more positive than the standard redox potential of E ($^{\bullet}OH/H_2O$) (+2.72 eV *vs.* NHE), indicating that H_2O could be oxidized to generate $^{\bullet}OH$. Therefore, the Z-scheme charge transfer mechanism was more reasonable for the TC degradation process.

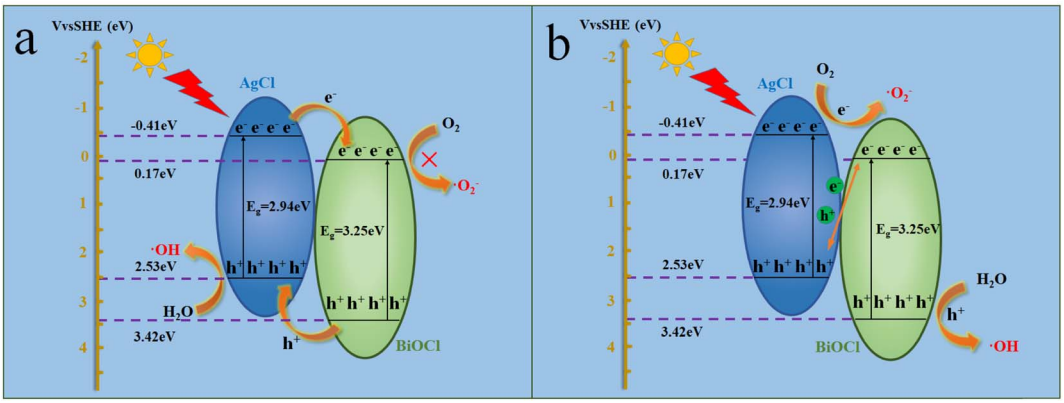

Fig. 15 Proposed photocatalytic mechanisms for the removal of TC over the AgCl/BiOCl heterojunction (a and b).

4 Conclusions

In summary, a Z-scheme AgCl/BiOCl heterojunction with oxygen vacancies was fabricated by the water-bath method. The as-synthesized AB heterojunction showed excellent photocatalytic activity for the degradation of TC and bacterial inactivation. The TC was degraded by 82% within 60 min, and the bacteria were inactivated within 60 min in the presence of the AB heterojunction. The enhanced photocatalytic degradation and disinfection efficiency could be attributed to the synergistic effect of the enhanced light absorption and effective photoinduced charge carrier separation and transfer through the construction of the Z-scheme AgCl/BiOCl heterojunction. In addition, environmental factor experiments have shown that high concentrations of TC, low catalyst doses, and PO_4^{3-} could reduce the photocatalytic degradation efficiency of the AB heterojunction. The degradation efficiency of the AB heterojunction on ofloxacin, norfloxacin, and Lanasol Red 5B was 73.52%, 74.37%, and 96.13%, respectively. The trapping experiment indicated that $^{\cdot}O_2^-$ was the main active species for TC degradation and bacterial inactivation. Based on capture experiments and band analysis, it was inferred that the AB heterojunction belonged to a Z-scheme heterojunction.

Conflicts of interest

The authors declare that they have no known competing financial interests or personal relationships that could have appeared to influence the work reported in this paper.

Acknowledgements

The study was supported by the Key Research and Development Project of Henan Province (Grant No. 221111321500), Natural Science Foundation of Henan Province (Grant No. 232300420358), Scientific and Technological Project in Henan Province (Grant No. 222102320376 and 232102320102) and Doctor Initiated Project of Luoyang Institute of Science and Technology (Grant No. 21010707).

References

1 X. Yan, Q. Ji, C. Wang, J. Xu and L. Wang, In situ construction bismuth oxycarbonate/bismuth oxybromide Z-scheme heterojunction for efficient photocatalytic removal of tetracycline and ciprofloxacin, *J. Colloid Interface Sci.*, 2021, **587**, 820–830.
2 P. Wang and Q. Yuan, Photocatalytic degradation of tetracyclines in liquid digestate: Optimization, kinetics and correlation studies, *Chem. Eng. J.*, 2021, **410**, 128327.
3 H. Liu, S. Ma, L. Shao, H. Liu, Q. Gao, B. Li, H. Fu, S. Fu, H. Ye, F. Zhao and J. Zhou, Defective engineering in graphitic carbon nitride nanosheet for efficient photocatalytic pathogenic bacteria disinfection, *Appl. Catal., B*, 2020, **261**, 118201.
4 H. Qiu, S. Fang, G. Huang and J. Bi, A novel application of $In_{(2)}S_{(3)}$ for visible-light-driven photocatalytic inactivation of bacteria: Kinetics, stability, toxicity and mechanism, *Environ. Res.*, 2020, **190**, 110018.
5 A. Zhu, S. Ali, Z. Wang, Y. Xu, R. Lin, T. Jiao, Q. Ouyang and Q. Chen, ZnO@Ag-functionalized paper-based microarray chip for SERS detection of bacteria and antibacterial and photocatalytic inactivation, *Anal. Chem.*, 2023, **95**, 18415–18425.
6 A. Akhundi, A. Habibi-Yangjeh, M. Abitorabi and S. Rahim Pouran, Review on photocatalytic conversion of carbon dioxide to value-added compounds and renewable fuels by graphitic carbon nitride-based photocatalysts, *Catal. Rev.*, 2019, **61**, 595–628.
7 D. Zhang, S. Liang, S. Yao, H. Li, J. Liu, Y. Geng and X. Pu, Highly efficient visible/NIR photocatalytic activity and mechanism of $Yb3^+/Er^{3+}$ co-doped $Bi_4O_5I_2$ up-conversion photocatalyst, *Sep. Purif. Technol.*, 2020, **248**, 117040.
8 S. Fu, W. Yuan, X. Liu, Y. Yan, H. Liu, L. Li, F. Zhao and J. Zhou, A novel 0D/2D WS_2/BiOBr heterostructure with rich oxygen vacancies for enhanced broad-spectrum photocatalytic performance, *J. Colloid Interface Sci.*, 2020, **569**, 150–163.
9 Y. Cai, D. Li, J. Sun, M. Chen, Y. Li, Z. Zou, H. Zhang, H. Xu and D. Xia, Synthesis of BiOCl nanosheets with oxygen

vacancies for the improved photocatalytic properties, *Appl. Surf. Sci.*, 2018, **439**, 697–704.
10 S. Zhao, Y. Zhang, Y. Zhou, C. Zhang, X. Sheng, J. Fang and M. Zhang, Reactable polyelectrolyte-assisted synthesis of BiOCl with enhanced photocatalytic activity, *ACS Sustainable Chem. Eng.*, 2017, **5**, 1416–1424.
11 W. Liu, Q. Li, X. Yang, X. Chen and X. Xu, Synthesis of SiC/BiOCl composites and its efficient photocatalytic activity, *Catalysts*, 2020, **10**, 946.
12 C. Guan, T. Hou, W. Nie, Q. Zhang, L. Duan and X. Zhao, Sn^{4+} doping enhanced inner electric field for photocatalytic performance promotion of BiOCl based nanoflowers, *Appl. Surf. Sci.*, 2022, **604**, 154498.
13 D. Zhang, C. Su, S. Yao, H. Li, X. Pu and Y. Geng, Facile in situ chemical transformation synthesis, boosted charge separation, and increased photocatalytic activity of $BiPO_4$/BiOCl p–n heterojunction photocatalysts under simulated sunlight irradiation, *J. Phys. Chem. Solids*, 2020, **147**, 109630.
14 C. Guan, T. Hou, W. Nie, Q. Zhang, L. Duan and X. Zhao, Boosting visible light driven gas–solid phase photocatalytic reduction of CO_2 on BiOCl microspheres by enhanced carrier transportation through lattice structure modification, *Sep. Purif. Technol.*, 2023, **306**, 122654.
15 X. Xu, N. Yang, P. Wang, S. Wang, Y. Xiang, X. Zhang, X. Ding and H. Chen, Highly intensified molecular oxygen activation on $Bi@Bi_{(2)}MoO_{(6)}$ via a metallic Bi-coordinated facet-dependent effect, *ACS Appl. Mater. Interfaces*, 2020, **12**, 1867–1876.
16 N. Tian, C. Hu, J. Wang, Y. Zhang, T. Ma and H. Huang, Layered bismuth-based photocatalysts, *Coord. Chem. Rev.*, 2022, **463**, 214515.
17 A. Kundu, S. Sharma and S. Basu, Modulated BiOCl nanoplates with porous g-C3N4 nanosheets for photocatalytic degradation of color/colorless pollutants in natural sunlight, *J. Phys. Chem. Solids*, 2021, **154**, 110064.
18 X. Liu, X. Song, X. Jian, H. Yang, X. Mao and Z. Liang, A BiOCl/bipolar membrane as a separator for regenerating NaOH in water-splitting cells, *RSC Adv.*, 2016, **6**, 9880–9883.
19 J. Wang and Z. Zhang, Co-precipitation synthesis and photocatalytic properties of BiOCl microflowers, *Optik*, 2020, **204**, 164149.
20 W. Lin, X. Yu, Y. Shen, H. Chen, Y. Zhu, Y. Zhang and H. Meng, Carbon dots/BiOCl films with enhanced visible light photocatalytic performance, *J. Nanopart. Res.*, 2017, **19**, 56.
21 Y. Fang, G. Zhao, W. Dai, L. Ma and N. Ma, Enhanced adsorption of rubidium ion by a phenol@MIL-101(Cr) composite material, *Microporous Mesoporous Mater.*, 2017, **251**, 51–57.
22 R. B. Arthur, J. L. Bonin, L. P. Ardill, E. J. Rourk, H. H. Patterson and E. A. Stemmler, Photocatalytic degradation of ibuprofen over BiOCl nanosheets with identification of intermediates, *J. Hazard. Mater.*, 2018, **358**, 1–9.
23 Y. Peng, Y. G. Mao and P. F. Kan, One dimensional hierarchical BiOCl microrods: their synthesis and their photocatalytic performance, *CrystEngComm*, 2018, **20**, 7809–7817.
24 Z. Xu, Y. Gu, Y. An, C. Zhang, Y. Yu, A. Long and L. Huang, P123-modified synthesis of BiOCl nanosheet/bismuth nitrate heterojunctions for photocatalytic pollutant degradation, *ACS Appl. Nano Mater.*, 2021, **5**, 931–938.
25 K. Xie, S. Xu, K. Xu, W. Hao, J. Wang and Z. Wei, BiOCl Heterojunction photocatalyst: Construction, photocatalytic performance, and applications, *Chemosphere*, 2023, **317**, 137823.
26 X. Sun, J. Lu, J. Wu, D. Guan, Q. Liu and N. Yan, Enhancing photocatalytic activity on gas-phase heavy metal oxidation with self-assembled BiOI/BiOCl microflowers, *J. Colloid Interface Sci.*, 2019, **546**, 32–42.
27 W. Shi, M. Li, X. Huang, H. Ren, F. Guo, Y. Tang and C. Lu, Construction of $CuBi_2O_4/Bi_2MoO_6$ p–n heterojunction with nanosheets-on-microrods structure for improved photocatalytic activity towards broad-spectrum antibiotics degradation, *Chem. Eng. J.*, 2020, **394**, 125009.
28 D. Zhang, R. Zhang, J. Liu, X. Pu and P. Cai, 3D/2D $ZnIn_2S_4$/$BiFeO_3$ as S-scheme heterojunction photocatalyst for boosted visible-light hydrogen evolution, *J. Am. Ceram. Soc.*, 2023, **106**, 4785–4793.
29 J. Du, S. Ma, H. Liu, H. Fu, L. Li, Z. Li, Y. Li and J. Zhou, Uncovering the mechanism of novel $AgInS_2$ nanosheets/TiO_2 nanobelts composites for photocatalytic remediation of combined pollution, *Appl. Catal., B*, 2019, **259**, 118062.
30 L. Li, J. Cai, Y. Yan, F. Zhao and J. Zhou, Flower-like direct Z-scheme $WS_2/Bi_2O_2CO_3$ photocatalyst with enhanced photocatalytic activity, *J. Alloys Compd.*, 2019, **810**, 151872.
31 Z. Feng, J. Yu, D. Sun and T. Wang, Visible-light-driven photocatalysts Ag/AgCl dispersed on mesoporous Al_2O_3 with enhanced photocatalytic performance, *J. Colloid Interface Sci.*, 2016, **480**, 184–190.
32 B. Zhang, H. Zhang, D. Ma, F. Liang, H. Lan and F. Yan, g-$C(3)N_{(4)}$/Ag@AgCl with Z-scheme heterojunction and Ag electron bridge for enhanced photocatalytic degradation of tetracycline wastewater, *Environ. Sci. Pollut. Res. Int.*, 2023, **30**, 112462–112473.
33 H. Zhu, D. Chen, N. Li, Q. Xu, H. Li, J. He and J. Lu, Cyclodextrin-functionalized Ag/AgCl foam with enhanced photocatalytic performance for water purification, *J. Colloid Interface Sci.*, 2018, **531**, 11–17.
34 J. Wu, X. Fang, H. Dong, L. Lian, N. Ma and W. Dai, Bimetallic silver/bismuth-MOFs derived strategy for Ag/AgCl/BiOCl composite with extraordinary visible light-driven photocatalytic activity towards tetracycline, *J. Alloys Compd.*, 2021, **877**, 160262.
35 M. Du, S. Zhang, Z. Xing, Z. Li, J. Yin, J. Zou, Q. Zhu and W. Zhou, All-solid Z-scheme Bi-BiOCl/AgCl heterojunction microspheres for improved electron-hole separation and enhanced visible light-driven photocatalytic performance, *Langmuir*, 2019, **35**, 7887–7895.
36 X. Guo, J. Liu, D. Li, H. Cheng, K. Liu, X. Liu and T. Liu, Facile construction of Z-scheme $AgCl/Bi_{(3)}TaO_{(7)}$ photocatalysts for effective removal of tetracycline under

visible-light irradiation, *Environ. Sci. Pollut. Res. Int.*, 2023, **30**, 62312–62324.

37 Y. Liu, J. Pan, W. Ou, P. Wang, Z. Chen and C. Li, Two dimensional Z-scheme $AgCl/Ag/MnTiO_3$ nano-heterojunctions for photocatalytic degradation performance enhancement, *IOP Conf. Ser. Earth Environ. Sci.*, 2019, **358**, 052013.

38 Z. Miao, Q. Wang, Y. Zhang, L. Meng and X. Wang, In situ construction of S-scheme AgBr/BiOBr heterojunction with surface oxygen vacancy for boosting photocatalytic CO_2 reduction with H_2O, *Appl. Catal., B*, 2022, **301**, 120802.

39 L. Li, Y. Yan, J. Du, S. Fu, H. Liu, F. Zhao and J. Zhou, Glucose-assisted hydrothermal synthesis of plasmonic Bi deposited nested $Bi_2O_2{-}xCO_3$ photocatalysts with enhanced photocatalytic activity, *Colloids Surf., A*, 2019, **583**, 123946.

40 S. Fu, Y. Du, J. Bie, Z. Huang, H. Hu, Q. Huang, H. Zhu, W. Yuan, L. Li and B. Liu, Facile fabrication of Z-scheme Ag_2WO_4/BiOBr heterostructure with oxygen vacancies for improved visible-light photocatalytic performance, *J. Sci.: Adv. Mater. Devices*, 2023, **8**, 100561.

41 Z. Wu, J. Jing, K. Zhang, W. Li, J. Yang, J. Shen, S. Zhang, K. Xu, S. Zhang and Y. Zhu, Epitaxial BiP_5O_{14} layer on BiOI nanosheets enhancing the photocatalytic degradation of phenol via interfacial internal-electric-field, *Appl. Catal., B*, 2022, **307**, 121153.

42 S. Fu, W. Yuan, Y. Yan, H. Liu, X. Shi, F. Zhao and J. Zhou, Highly efficient visible-light photoactivity of Z-scheme $MoS_{(2)}/Ag_{(2)}CO_{(3)}$ photocatalysts for organic pollutants degradation and bacterial inactivation, *J. Environ. Manage.*, 2019, **252**, 109654.

43 J. Lv, K. Dai, J. Zhang, L. Lu, C. Liang, L. Geng, Z. Wang, G. Yuan and G. Zhu, In situ controllable synthesis of novel surface plasmon resonance-enhanced $Ag_2WO_4/Ag/Bi_2MoO_6$ composite for enhanced and stable visible light photocatalyst, *Appl. Surf. Sci.*, 2017, **391**, 507–515.

44 X. Wang, K. Maeda, A. Thomas, K. Takanabe, G. Xin, J. M. Carlsson, K. Domen and M. Antonietti, A metal-free polymeric photocatalyst for hydrogen production from water under visible light, *Nat. Mater.*, 2009, **8**, 76–80.

45 H. Zhang, W. Zhao and H. Shi, Oxygen vacancy-rich 2D/0D $BiO_{(1-X)}Br$/AgBr Z-scheme photocatalysts for efficient visible light driven degradation of tetracycline, *Nanotechnology*, 2021, **32**, 43.

46 J. Chen, G. Li, N. Lu, H. Lin, S. Zhou and F. Liu, Anchoring cobalt single atoms on 2D covalent triazine framework with charge nanospatial separation for enhanced photocatalytic pollution degradation, *Mater. Today Chem.*, 2022, **24**, 100832.

47 G. Zhang, X. He, M. N. Nadagouda, K. E. O'Shea and D. D. Dionysiou, The effect of basic pH and carbonate ion on the mechanism of photocatalytic destruction of cylindrospermopsin, *Water Res.*, 2015, **73**, 353–361.

48 S. Li, J. Chen, S. Hu, H. Wang, W. Jiang and X. Chen, Facile construction of novel Bi_2WO_6/Ta_3N_5 Z-scheme heterojunction nanofibers for efficient degradation of harmful pharmaceutical pollutants, *Chem. Eng. J.*, 2020, **402**, 126165.

49 M. Li, C. Lai, H. Yi, D. Huang, L. Qin, X. Liu, B. Li, S. Liu, M. Zhang, Y. Fu, L. Li, J. He, Y. Zhang and L. Chen, Multiple charge-carrier transfer channels of Z-scheme bismuth tungstate-based photocatalyst for tetracycline degradation: Transformation pathways and mechanism, *J. Colloid Interface Sci.*, 2019, **555**, 770–782.

50 H. Zhang, Y. Liu, H. Liu, J. Yin, L. Shi and H. Tang, Surface anchoring of nickel sulfide clusters as active sites and cocatalysts for photocatalytic antibiotic degradation and bacterial inactivation, *J. Colloid Interface Sci.*, 2023, **637**, 421–430.